Journal of Alloys and Compounds 509 (2011) 6163–6169

Contents lists available at ScienceDirect

Journal of Alloys and Compounds

journal homepage: www.elsevier.com/locate/jallcom

Peculiar effects of microwave sintering on ZnO based varistors properties

Etienne Savary[a,*], Sylvain Marinel[a], Franck Gascoin[a], Yoshiaki Kinemuchi[b], Julien Pansiot[c], Richard Retoux[a]

[a] Laboratoire CRISMAT, 6 Bd. Maréchal Juin, 14050 Caen Cedex 4, France
[b] National Institute of Advanced Industrial Science and Technology (AIST), Nagoya 463-8560, Japan
[c] Laboratoire Interdisciplinaire Carnot de Bourgogne, 9 Av. Alain Savary, 21078 Dijon Cedex, France

ARTICLE INFO

Article history:
Received 5 January 2011
Received in revised form 1 March 2011
Accepted 6 March 2011
Available online 12 March 2011

Keywords:
Zinc oxide
Varistors
Microwaves
Electrical properties
Nanoparticles
Microstructures

ABSTRACT

Non-ohmic properties of doped zinc oxide are widely used in varistors applications. It is well established that final properties of the component are strongly correlated with reactivity of the added phases during sintering process and with final microstructure. In this paper, the specific effects of the hybrid single-mode microwave sintering process on the microstructure and electrical properties of a ZnO-based composition are investigated. Nano-sized ZnO-based powder with a proper amount of Bi_2O_3, Sb_2O_3, CoO and MnO is synthesized by a liquid route and is sintered within a short time (less than 10 min) in a conventional (CV) or by an hybrid single-mode microwave (MW) furnaces. Distinct differences can be seen in the density, reaction kinetics and dopant diffusivity: higher kinetics of MW leads to denser pellet, faster reaction among dopants and faster diffusion of cobalt and manganese into ZnO grains although grain sizes are almost identical between CV and MW. These differences in terms of chemistry and microstructure lead to sharp contrasts in electrical properties.

1. Introduction

Zinc oxide is a well known functional material widely spread in various application fields, like for instance in electronic, optic and spintronic. Among them, the main application is ZnO-based varistors which are used as surge protectors in electrical circuits in either low or high voltage. ZnO is a direct band gap semiconductor [1] which exhibits a non linear current–voltage response, depending on both the processing conditions and the added dopants [2]. This typical electrical response is known to be provided by the addition of dopants like Bi_2O_3, Sb_2O_3, CoO or MnO [3]. Some of these dopants, like Bi_2O_3 and Sb_2O_3, react with each other resulting in inter-granular secondary phases whereas others, like Co and Mn, coming from the added oxides, go into solution in ZnO grains [4]. Consequently, a p-type semiconducting area is formed in the vicinity of the grain boundaries while the core of the ZnO grain is n-type. Thus a double Schottky barrier is formed between two ZnO grains, which is responsible for the varistor non-ohmic response [5–7]. It is well understood that microstructure, including doping element distribution and grains size, has a strong influence on the ZnO electrical properties. After the finding of the non-linear properties in this system by Matsuoka in 1969, many investigations have been carried out to unveil the relationships among the starting composition and/or the processing conditions and the electrical properties. One can mention the influence of vibratory milling [8,9], sintering and annealing conditions [10,11]. Different synthesis methods have also been investigated such as precipitation [12,13], solution-coating [14], sol–gel [15], combustion [16] and self-propagating high-temperature [17] methods. Contrariwise, only few works report the effect of a fast sintering process, like microwave sintering, on the microstructure and properties of ZnO based varistors. Leach et al. have studied the local microstructure and the functional property of ZnO sintered by a microwave-assisted process [18], using a conventional heating furnace combined with microwaves radiation. With similar heating program, the microwave assisted heating process leads to similar grain size but slightly higher density over conventional process. Although electrical responses measured through the bulk are similar, local electrical properties showed that spatial variations in non-linear coefficient and leakage current density were significantly reduced in the microwave assisted sintered samples. It is thus suggested that microwaves promote diffusion leading to more homogeneous Bi distribution than in conventionally sintered specimens. Subasri et al. have also investigated the indirect microwave sintering on suitably doped ZnO nano-powder [19] using multimode microwave cavity equipped with SiC rods as susceptors. In their study, they showed that microwave sintered samples exhibit finer grain size and higher density than those obtained on conventionally sintered samples, with similar temperature profiles. Another study [20] reported that microwave sintering in

* Corresponding author. Tel.: +33 2 31 45 13 69; fax: +33 2 31 45 13 09.
E-mail address: etienne.savary@ensicaen.fr (E. Savary).

0925-8388/$ – see front matter © 2011 Elsevier B.V. All rights reserved.
doi:10.1016/j.jallcom.2011.03.048

single-mode cavity enhances densification of ZnO based varistors as well as grain growth, leading to degraded properties for long time sintered samples. The enhancement of densification is reported by many works however some contradictory results on grain growth are observed. In fact, the comparison of the results of the literature leads to a misunderstanding due to the different microwave furnaces used (choice of susceptor and microwave mode). The goal of this work is to clarify this issue: the effects of microwave irradiation on the microstructure (grain growth), dopants diffusion and resultant electrical properties of nano-sized based ZnO varistors. To get a temperature distribution as homogenous as possible, hybrid microwave sintering in single mode cavity was designed using a rectangular 2.45 GHz cavity and a cylindrical ZnO susceptor. As comparison, the conventional sintering was also performed with similar short sintering time (<10 min). A conventional sintering experiment with usual temperature–time profiles was also carried out as a reference. Macrostructure observations and chemical analysis were performed and discussed according to the electrical response and Shottky barriers properties in order to understand the peculiar effects of microwave processing.

2. Experimental procedure

2.1. Synthesis, powder characterization and shaping

The liquid route synthesis developed for the preparation of the varistors is described by Fig. 1. Zinc acetate (Chempur, 99.5%) was first dissolved in absolute ethanol and the dopants were added to the solution from metal oxides powders in proportion of 98 mol% ZnO, 0.5 mol% Bi_2O_3, 0.5 mol% Sb_2O_3, 0.5 mol% CoO, 0.5 mol% MnO. The resulting solution was stirred during 1 h at 70 °C to achieve a good dissolution of the precursors. An oxalic acid solution was then poured leading to the precipitation of the zinc oxalate. The latter was dried under infrared lamps and calcined in air at 400 °C for 1 h to get the zinc oxide based powder [21]. The crystalline phases were identified by X-Ray Diffraction (XRD) using Cu Kα radiation (Philips X'Pert diffractometer). The electron diffraction and the Transmission Electron Microscopy (TEM) observations of the nanoparticles were performed at room temperature on 200 kV JEOL 2010 FEG electron microscopes (tilt ±60° and ±42°). This microscope is equipped with double tilt sample holders (tilt ±25°). A few droplets of suspension in absolute ethanol were deposited on nickel holey carbon grid. The specific surface area was determined by the BET method based on nitrogen adsorption. For the shaping, an organic binder (Rhodoviol 4%, Prolabo) was manually added to the powder and disks (6.4 mm in diameter, 1.3 mm in thickness) were shaped using a 30.6 kN uniaxial load.

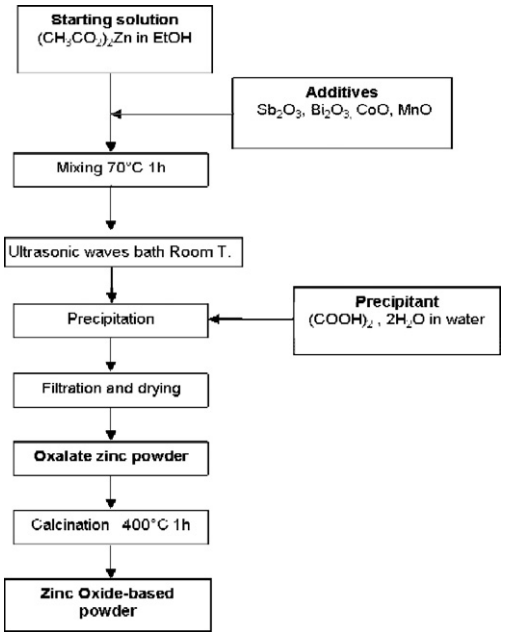

Fig. 1. Flowchart of the liquid route synthesis of ZnO based nano-powder.

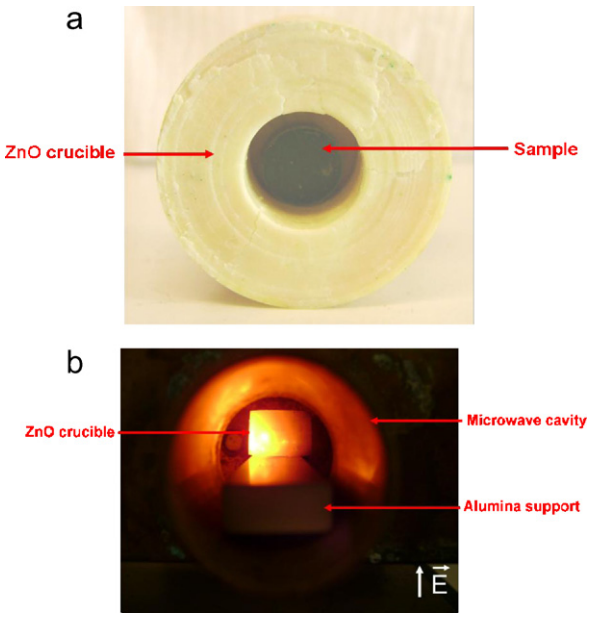

Fig. 2. (a) Picture of the ZnO based sample located in a crucible made from ZnO and used as susceptor and (b) picture of the ZnO crucible susceptor heated in the microwave cavity.

2.2. Microwave equipment

The microwave furnace consists of a microwave generator (2.45 GHz Sairem GMP20KSM) delivering a variable power of up to 2000 W. The microwave radiation passes through a rectangular waveguide (WR340) ended by a TE10p cavity. A coupling iris and a short circuit piston allow to tune the cavity either in the TE102 mode or in the TE103 mode. The sample is positioned in the centre of the cavity in a ZnO cylindrical crucible whose axis is perpendicular to the electric field (Fig. 2) [22]. The crucible was made from ZnO so as to avoid any contamination of the sample by the crucible. Using this hybrid heating configuration, the sample is surrounded by a warm environment in order to reduce the thermal radiation from the sample surface and improve the homogeneity of the temperature distribution in the sample. This configuration also allows to achieve good thermal conditions reproducibility.

2.3. Microwave and conventional sintering

Before microwave and fast conventional sintering, a first heating treatment was carried out in a conventional furnace at 400 °C for 1 h to remove the organic binder. The microwave sintering was performed in air at three dwell powers (500 W, 550 W, 600 W), with 5 min dwell time. The incident power was increased by 100 W every 30 s up to the dwell power for simulating a heating ramp (Fig. 3). During the dwell step, the maximum and stable temperature was measured on the sample surface by infrared thermometer (Modline 5 model). To analyse if whether or not microwaves have a peculiar effect on the ZnO based varistors properties, conventional sintering was also performed in the same temperature range than for MWs samples, and with a similar dwell time (Table 1). The short conventional sintering being carried out without any heating ramp (the sample is directly introduced into the furnace previously programmed at dwell temperature), a slightly longer dwell time has been applied (i.e., 9 min) compared to the MW cycle (i.e., 5 min) considering heating ramp

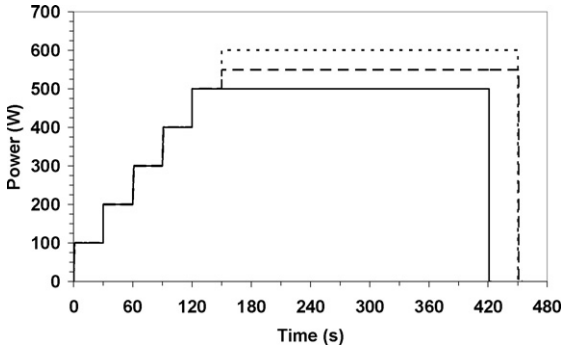

Fig. 3. Incident power versus time used for the microwave sintering.

Table 1
Sample references and their sintering conditions.

Conventional sintering – reference			
Sintering parameters		1100 °C 1 h	
Sample reference		CV	
Microwave sintering			
Sintering parameters	500 W 5 min	550 W 5 min	600 W 5 min
Surface temperature	1145 °C	1175 °C	1200 °C
Sample reference	MW1	MW2	MW3
Fast Conventional sintering			
Sintering parameters	1100 °C 9 min	1200 °C 9 min	1250 °C 9 min
Sample reference	CV F1	CV F2	CV F3

during MW process. It is thus reasonable to claim that in both processes, samples are subjected at dwell temperatures for similar periods. To set up a reference, one sample has been sintered in conventional conditions using usual time–temperature profile: heating and cooling ramps 150 °C/h and dwell time of 1 h (Table 1).

2.4. Sintered samples characterization

The microstructures of the sintered samples were observed by SEM (SEM Supra 55 from Zeiss). The samples for TEM observations were prepared by crushing bulk sintered pellets in absolute ethanol. The local chemical composition (in the grains cores and grain boundaries) was investigated using Energy Dispersive Spectroscopy (EDS) analysers coupled with TEM. The JEOL 2010 FEG electron microscope is equipped with the system EDAX Genesis.

Electric field–current density (E–J) characteristic of the varistors was measured at room temperature using a Keithley 237 unit. Both faces of the samples were coated with silver paste and ohmic contacts were formed by a heat treatment at 900 °C. The breakdown electric field (E_b) was then determined for a current density of 1 mA/cm^2 and the leakage current density (J_L) was defined as the current density at 0.8 E_b. The nonlinear coefficient was calculated from: $\alpha = (\log J_2 - \log J_1)/(\log E_2 - \log E_1)$ with $J_2 = 10$ mA/cm^2 and $J_1 = 1$ mA/cm^2.

The capacitance–voltage (C–V) characteristic of the samples was measured at 1 kHz using a RLC meter (Fluke PM6306) and a DC bias voltage source (Metrix AX 322). The donor concentration (N_d) was determined by the slope of the graph: $(1/C_b - 1/C_{b0})^2 = 2(\phi + V_{gb})/q\varepsilon_0\varepsilon_r N_d$ [23] where V_{gb} is the applied voltage per grain boundary, ϕ is the barrier height, C_b is the capacitance per unit area of a grain boundary, C_{b0} is the value of C_b when $V_{gb} = 0$, q the electronic charge, ε_0 the vacuum permittivity, ε_r the ZnO relative permittivity ($\varepsilon_r = 8.5$). From the SEM micrographs, the grains average size was determined by the Mendelson's method [24] considering the average grain size G as: $G = 1.56 \times L$ with L the average length between grains. The density of interface states (N_t) at the grain boundary was then calculated by the equation: $N_t = (2\varepsilon N_d \phi/q)^{1/2}$ [23].

3. Results and discussion

3.1. Zinc oxide powder synthesis

Zinc oxide based powder was successfully synthesized as shown by the XRD pattern (Fig. 4). It is also shown that the Bi_2O_3 phase is detected, but among all the added phases (Bi_2O_3, Sb_2O_3, CoO, MnO), it is the only one that can be identified. Using TEM (Fig. 5a), the ZnO particles appear to be nano-crystalline with a nearly spherical shape and a very narrow particle size distribution. The BET specific surface area of the powder is 53 m^2/g. An estimated value of the grain diameter (d) of 19 nm is deduced using the equation $d = 6000/\rho S$, assuming spherical and mono-dispersed powder, in which ρ is the theoretical density (5.66 g/cm^3), and S, the specific surface area. This calculated diameter, at the nano-metric scale, is consistent with both the broad width of the XRD peaks and the TEM observation. Moreover, on the High-Resolution TEM image (HRTEM), the characteristic contrasts of a well crystallized phase were also evident (Fig. 5b). From the diffraction pattern (Fig. 6), the unit cell parameters are $a = b = 3.242$ Å, $c = 5.176$ Å, $\gamma = 120°$ (space group $P6_3mc$, n°186) which are in good agreement with the value reported for ZnO [25]. A simulated XRD pattern is also superposed in this figure showing a good agreement between the experimental and the theoretical patterns.

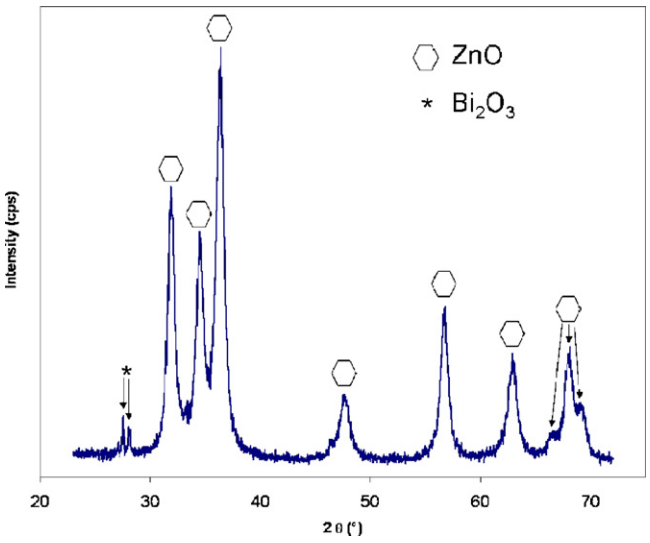

Fig. 4. XRD pattern of the zinc oxide based nano-powder synthesized by the oxalate liquid route.

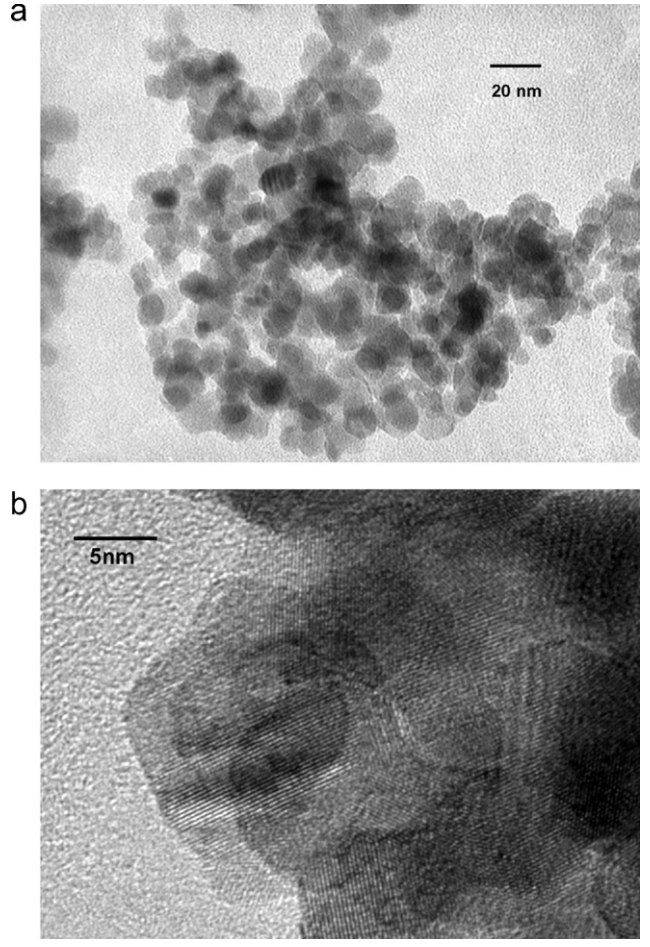

Fig. 5. (a) TEM and (b) HRTEM images of the nano-powder synthesized by the liquid route.

3.2. Conventional and microwave sintering

The nomenclature of sintered samples is given in Table 1. The geometrical densities obtained after the sintering cycles are shown in Table 2. It can be noticed that the relative density of the

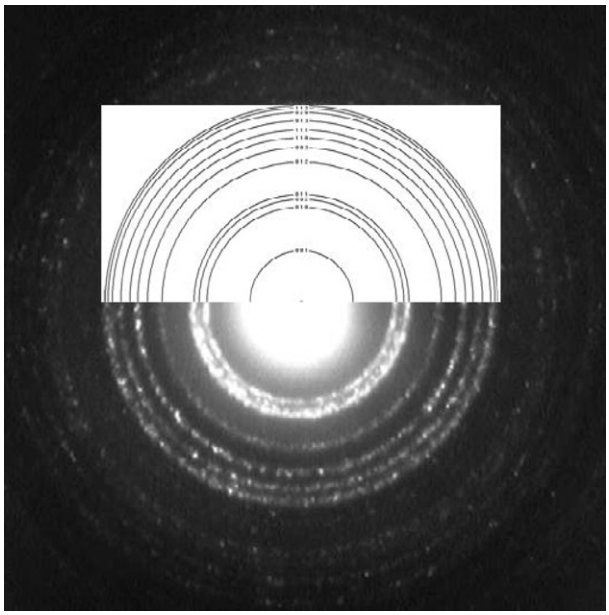

Fig. 6. Selected area electron diffraction patterns of a ZnO nanoparticle agglomerate with typical rings of diffraction spots. They well agree with calculated ED patterns (upper half).

Table 2
Density and average grain size of the ZnO based ceramics.

Sample reference	CV	MW1	MW2	MW3	CVF1	CVF2	CVF3
ρ(%)	94.9	92.8	97.1	98.6	83.8	84.4	83.1
d (μm) ± 1 μm	15	4	7	10	4.5	7	10.5

sample sintered in a conventional furnace (CV sample) during one hour is 94.9%, which is very close to the values of the samples sintered by microwaves. However, conventionally sintered samples with a short processing time (CV F samples) exhibit significantly lowered relative density, i.e. roughly 84%. It is noticeable that the temperature range used for microwave sintering [1145–1200 °C measured by calibrated IR Pyrometer, see Table 1] is comprised in the temperature range chosen for short conventional sintering [1100–1250 °C measured by thermocouple]. It is thus reasonable to think that the sample temperature during microwave heating cannot exceed the maximum temperature used for CV F3 sample (1250 °C). In the same manner, the minimum sintering temperature for MW heating is reasonably higher than the minimum temperature set for CV F1, i.e. 1100 °C. Although there is a certain uncertainty of temperature measurement in microwaves, the hybrid set up used in the present study must likely lower it. In spite of the small difference in firing temperature, microwave heating enhances densification as clearly evidenced by the final densities as shown in Table 2. This phenomenon can be explained by the difference in penetration depth between infra-red and microwaves. Because of the rather shallow penetration depth of infra-red, the surface temperature tends to be higher, leading to retardation of shrinkage caused by the inhomogeneous heating. At the contrary, microwaves penetrate through the sample, resulting in uniform temperature distribution and higher density. In addition, our hybrid heating setup promotes the uniform temperature distribution, in which infra-red heating (from susceptor) and microwaves heating of the sample, simultaneously take place.

Fig. 7 provides typical microstructures of sintered samples. First of all, it is obvious that, at a given holding time, the sintering temperature governs the grain size (Table 2). Since there is no noticeable grain size difference between MW and CV F samples,

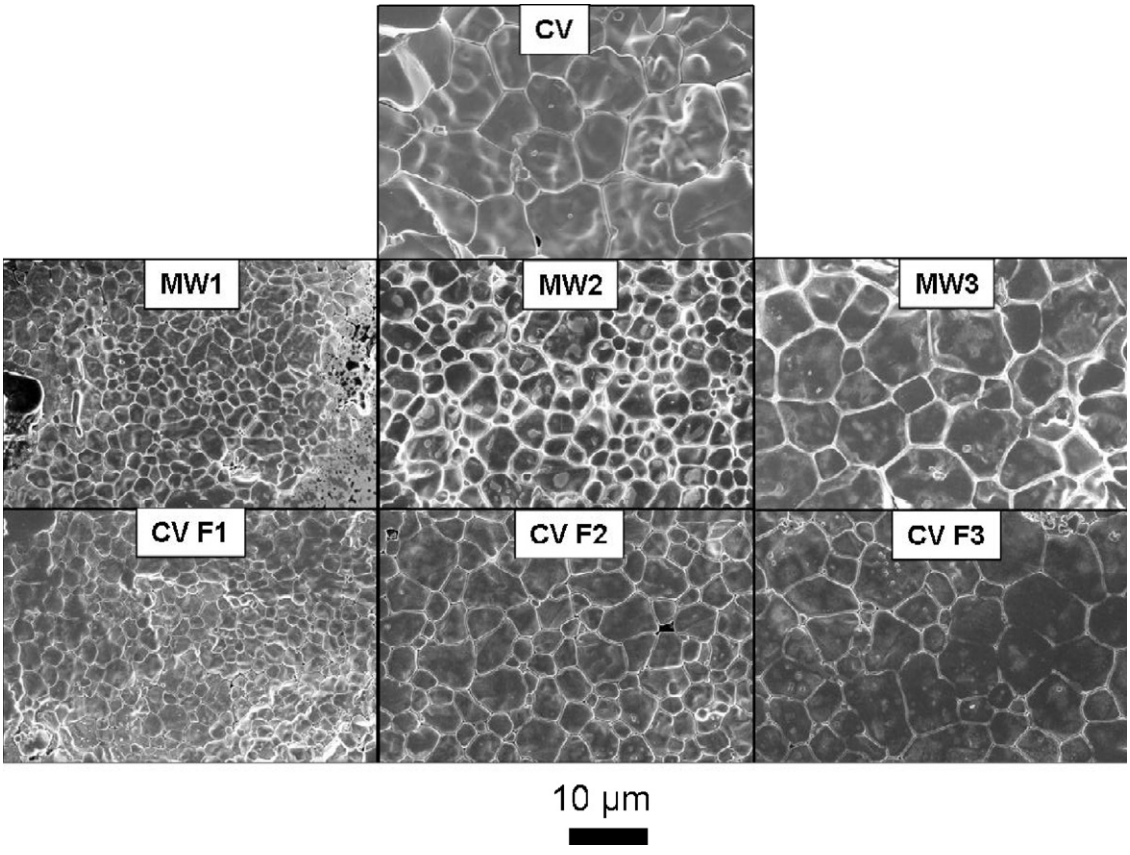

Fig. 7. SEM micrographs of the ZnO based ceramics.

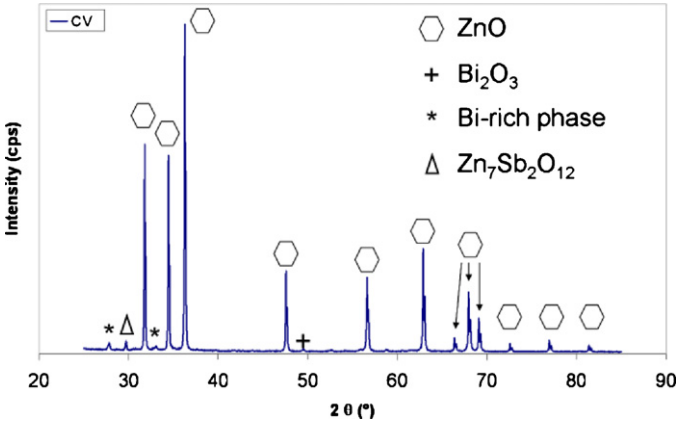

Fig. 8. XRD pattern of the varistor CV.

it is reasonable to assume that the grain growth is mostly governed by the amount of energy rather than by the way the energy is transferred.

Fig. 8 shows a typical powder XRD pattern (recorded on CV sample). ZnO (PDF#01-089-0511, main phase), Bi_2O_3 (PDF#00-002-0988), Bi-rich phase derived from Bi_2O_3 (see the main peak at $2\theta = 27.5^\circ$) and the spinel type phase $Zn_7Sb_2O_{12}$ were detected. For all the sintering methods, no other crystallized phase has been identified. However, difference in the phase content was found depending on the process. An important difference can be noticed concerning the reactivity of the Bi_2O_3 precursor phase. It is reported that the Bi_2O_3 phase reacts with ZnO and Sb_2O_3 phases to form the pyrochlore phase $Bi_3Zn_2Sb_3O_{14}$ (at 600–700 °C) [26]. Further, the $Bi_3Zn_2Sb_3O_{14}$ pyrochlore phase decomposes into $Zn_7Sb_2O_{12}$ spinel type phase (main peak at $2\theta = 29.5^\circ$) and Bi-rich phase (main peak at $2\theta = 27.5^\circ$) at higher temperatures. Those phases were clearly observed in all samples. Fig. 9 represents the magnified XRD patterns (from $2\theta = 45^\circ$ to $2\theta = 51^\circ$) in which the main peak of the unreacted Bi_2O_3 phase is observed at about $2\theta = 49.5^\circ$. The relative intensities between the Bi_2O_3 peak ($2\theta = 47.5^\circ$) and the ZnO peak allow us to follow up the progress of the pyrochlore formation. The CV F and MW samples show evident trace of Bi_2O_3 phase because of their short holding time, and the relative intensity ratio is weaker for the MW despite identical holding time (the ratio $I_{Bi_2O_3}/I_{ZnO}$ is 0.13 for CV F2 sample and 0.08 for MW3 sample), suggesting enhanced kinetics of the pyrochlore formation via microwaves. Local EDS analyses, from TEM investigations, have been performed on samples sintered by both methods. The Co and Mn atoms are clearly evidenced as traces in ZnO grain for CV reference and MW series as demonstrated in the typical EDS spectra (Fig. 10). Within the detection limit of EDS analysis, we could not find any trace of Co and Mn in ZnO grain for CV F samples. These results suggest that MW process enhances dopant diffusion. Possibly, additional external field, i.e. electromagnetic fields, promotes solid state diffusion. Phenomenon such as electromigration or field induced pressure [27] could be assumed. Moreover, Bi_2O_3 well-known absorber of microwave radiations [28], hence possibly subjected to higher temperatures than the whole sample, is likely to contribute to the rapid synthesis and diffusion for MW samples. Similar trend is observed for donor concentrations as discussed later.

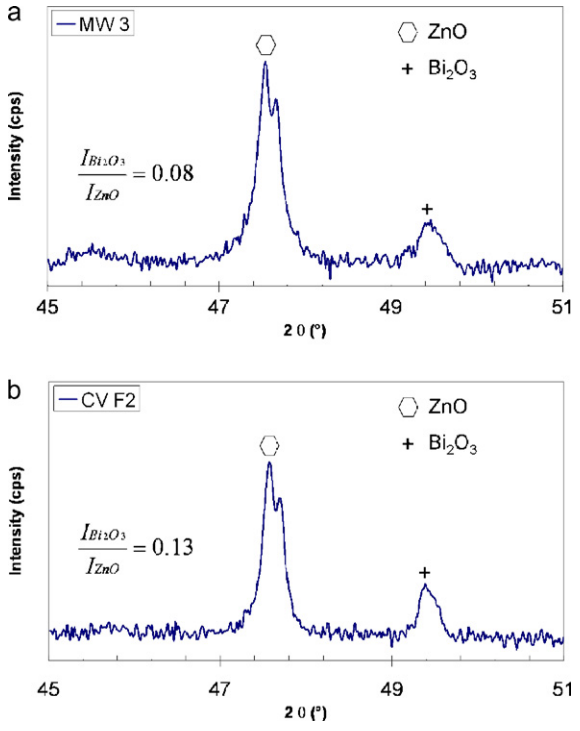

Fig. 9. XRD patterns scaling from $2\theta = 45^\circ$ to $2\theta = 51^\circ$ of the sintered samples: (a) CV F2 and (b) MW3. In inclusion, peaks intensity ratio between ZnO and Bi_2O_3 ($I_{ZnO}/I_{Bi_2O_3}$) are also shown.

Table 3
Breakdown electric field (E_b), leakage current density (J_L) and non-linear coefficient (α) of the varistors.

Sample reference	E_b (V/mm) ± 2 V/mm	J_L (mA/cm²) ± 0.005 mA/cm²	$a \pm 0.2$
CV	132	0.090	10.6
MW1	396	0.080	14.2
MW2	335	0.085	14.0
MW3	315	0.095	12.2
CVF1	575	0.345	8.3
CVF2	548	0.201	13.7
CVF3	284	0.418	5.9

3.3. Electrical properties

Fig. 11a shows the simplified equivalent electrical circuit of a varistor type component. R_{GB} is the resistance of the intergranular layer and Cp corresponds to the equivalent capacitance of the intergranular layers (depletion layers). R_b is the equivalent bulk resistance of the ZnO grains. When the applied voltage is low, the resistivity of the intergranular layer is quite high and the current passing through the ceramics is low. Hence R_{GB} parameter governs the $E(J)$ response at low field. With an increasing voltage, the resistance R_{GB} decreases, and above a certain voltage, R_{GB} becomes lower than R_b and the $E(J)$ characteristic tends to become ohmic. In the high voltage region, the bulk resistance of the ZnO grain mainly affects the electrical response. Fig. 11b shows the $E(J)$ characteristics of all the samples. It can be seen that the CV reference and MW samples have similar $E(J)$ curves with a sharp transition from the low current zone to the non-linear region. All MW samples exhibit nonlinear coefficient values higher than 12 (i.e., slightly higher values than CV reference), showing that all these samples exhibit a varistor type behavior (Table 3). On the contrary, the CV F samples present low α values (less than 10 for CV F1 and CV F3). Unsatisfactory varistor type $J(E)$ characteristic of CV F can be understood by (i) a low R_{GB} resistance causing high leakage current and (ii) a high R_b value as indicated in steep $E(J)$ slope curve at high current density. The point (i) is consistent with microstructural analysis indicating that the short sintering time is not enough to synthesize resistive Bi-rich intergranular phases. The point (ii) can be related to the dopants migration, especially Co and Mn, into the ZnO grains with a short processing time, which will be discussed later. On

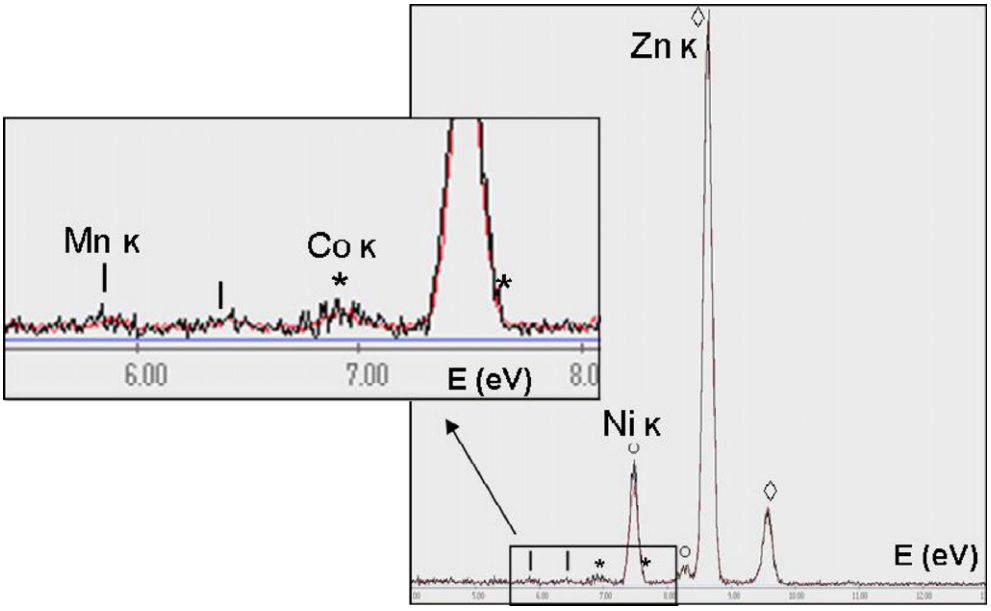

Fig. 10. Partial EDS spectra recorded on the ZnO grains' core between 5 and 13 eV of CV(in black line) and MW(in red line) samples. Note that Ni K characteristic peaks originate from the nickel grid supporting the samples. The two spectra are strictly identical. In inset, the Mn K and Co K lines, characteristic of the presence of few Mn and Co atoms (less than 1%), are slight but clearly evidenced.

Table 4
Donor concentration (N_d) and interface state density (N_t) of the varistors.

Sample reference	N_d (10^{14} cm^3)	N_t (10^{11} cm^2)
CV	86.5 ± 4.0	29.6 ± 1.5
MW1	10.6 ± 0.6	4.8 ± 0.3
MW2	17.1 ± 0.4	9.1 ± 0.5
MW3	8.3 ± 0.9	6.1 ± 0.4
CVF1	2.4 ± 0.2	3.0 ± 0.3
CVF2	5.2 ± 0.3	9.6 ± 0.7
CVF3	4.1 ± 0.1	8.0 ± 0.2

the contrary, in spite of short processing time, MW leads to usual varistor type $E(J)$ responses, i.e. a leakage current density around 80 μA/cm^2, a α value around 14 and a breakdown field ranging from 315 to 400 V/mm.

Focusing on the breakdown voltage, the samples sintered for a short time (MW and CV F samples) exhibit higher E_b values than CV sample (Table 3). The highest E_b is obtained for CV F1, for which E_b = 575 V/mm, which is more than four times the value of E_b for CV ($E_b \sim 130$ V/mm). This is obviously explained by the difference in grain size. That is small grain leads to a decrease in electric field at the grain boundary simply due to an increasing number of grain boundaries. However, despite a similar grain size between CV F and MW, CV F samples have higher E_b than MW samples because of a higher R_b.

From the $C(V)$ measurement, donor state concentration N_d and interface state density N_t have been calculated (Table 4). The highest N_d and N_t were observed for CV sample. These values are consistent with the fact that dopants have, in a large extent, reacted with the ZnO matrix. For MW and CV F sintered samples, both N_d and N_t values tend to be lower compared with CV, which may be caused by the short processing time. However, differences in N_d between CV F and MW samples are noticeable. In fact, the donor (Co and Mn) concentration is at least twice higher for MW samples. Furthermore, it is well established that such dopants are located at the grain boundary in the early stage of sintering before diffusing into the grains. So it can be suggested that the higher dopant concentration is due to enhanced dopant diffusion by MW irradiation. Thus it could be interesting in further studies to perform annealing of the MW sintered samples to increase the N_d and N_t values. The purpose

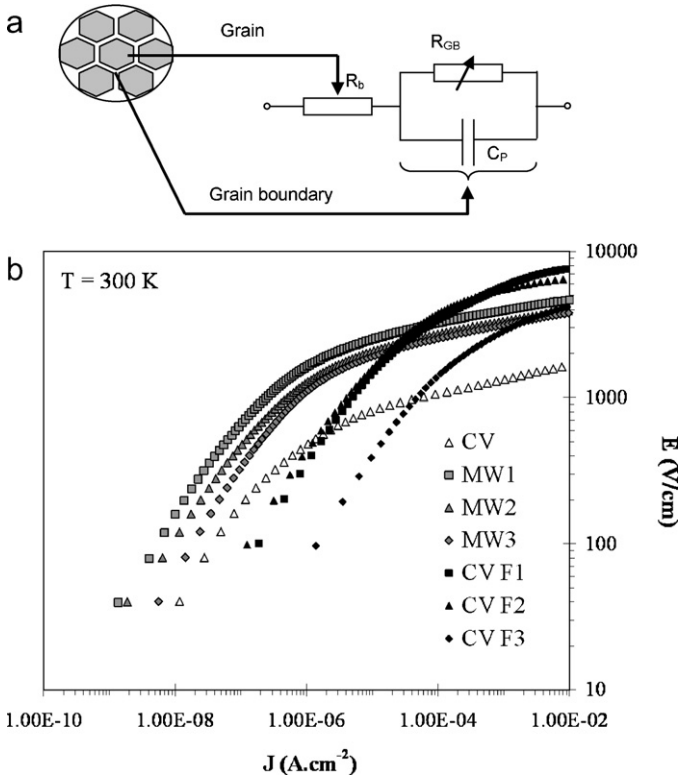

Fig. 11. (a) Simplified equivalent electrical circuit of a varistor type component and (b) E–J characteristics of the varistors.

of this annealing at low temperature (around 600 °C for instance) would be to favor dopants reaction with ZnO matrix while keeping fine grains. Specific characteristics of MW irradiated samples are illustrated in Fig. 12. Enhanced densification, better "interaction" matrix/dopants and higher dopant concentration are related to the unique features of MW processing: penetration depth, local heating and additional driving force for diffusion caused by electromagnetic fields.

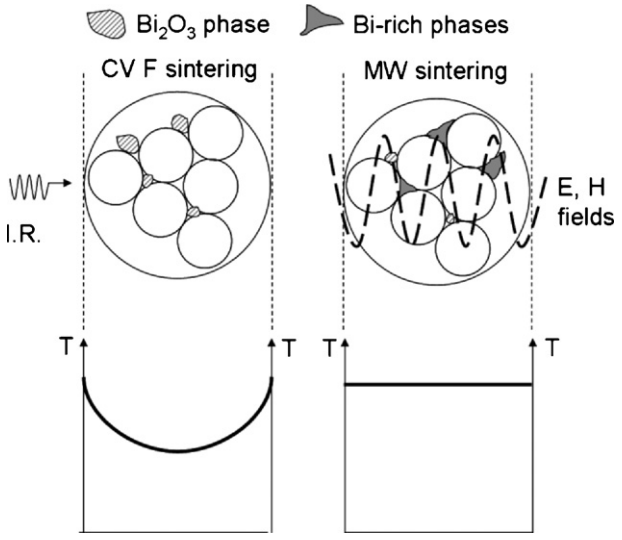

Fig. 12. Schematic depicting the reaction of the different phases and the temperature distribution through the samples sintered for a short time of heating in a conventional furnace and in a microwave furnace.

4. Conclusion

Starting from nano-sized ZnO powders, doped with usual additives for varistors, hybrid microwave sintering was performed and compared with fast conventional sintering. Sintered samples were thoroughly characterized in terms of structure, at different scales, and electrical properties, including the barrier characterization. Owing to a volumic heating process, it was clearly shown that microwave heating enhances the overall density. The grain growth follows the same trend with conventional way. On the contrary, the reaction kinetics between the different phases is enhanced by microwaves, which was confirmed by detailed analysis of the evolution of secondary phases and of electrical properties. Furthermore, faster dopant diffusion in microwaves is suggested from N_d measurements.

These 'microwave effects' may increase in the migration of atoms via peculiar phenomena such as electro migration or field induced pressure. A preferential microwave heating of the Bi_2O_3 phase could also be a likely explanation for microwaves enhanced reactivity phenomenon. From a practical point of view, the enhanced reactivity by microwaves opens new ways for producing faster and cheaper high performance functional ceramics.

Acknowledgements

Etienne Savary thanks the French Ministry of Research for the financial support. Yoshiaki Kinemuchi thanks JSPS for his financial support. The authors would like to thank Mrs François-Xavier Lefèvre, Jérôme Lecourt, Jacques Quillard, Stéphane Lejuez, Etienne Compagnon, Ms Alexandra Kennard and Isabelle Velluet for the technical support.

References

[1] U. Özgür, Y.I. Alivov, C. Liu, A. Teke, M.A. Reshchikov, S. Doğan, V. Avrutin, S. Cho, H. Morkoc, Journal of Applied Physics 98 (2005) 041301.
[2] L.M. Levinson, H.R. Philipp, Journal of Applied Physics 46 (1975) 1332.
[3] M. Matsuoka, Japanese Journal of Applied Physics 10 (1971) 736–746.
[4] C. Lin, W. Lee, C. Sun, W. Whu, Composites Part B: Engineering 38 (2007) 338–344.
[5] G. Pike, C. Seager, Journal of Applied Physics 50 (1979) 3414–3422.
[6] P. Mantas, J. Baptista, Journal of the European Ceramic Society 15 (1995) 605–615.
[7] G. Blatter, F. Greuter, Physical Review B 33 (1986) 3952.
[8] M. Kelleher, M. Hashmi, Journal of Materials Processing Technology 201 (2008) 645–650.
[9] S. Bernik, G. Brankovic, S. Rustja, M. Zunic, M. Podlogar, Z. Brankovic, Ceramics International 34 (2008) 1495–1502.
[10] C. Nahm, Materials Letters 60 (2006) 3394–3397.
[11] S. Jiang, H. Zhang, Y. Huang, M. Liu, R. Lin, Materials Science and Engineering B: Solid State Materials for Advanced Technology 117 (2005) 317–320.
[12] S. Anas, R. Mangalaraja, M. Poothayal, S. Shukla, S. Ananthakumar, Acta Materialia 55 (2007) 5792–5801.
[13] C. Chen, P. Liu, C. Lu, Chemical Engineering Journal 144 (2008) 509–513.
[14] Q. Wang, Y. Qin, G. Xu, L. Chen, Y. Li, L. Duan, Z. Li, Y. Li, P. Cui, Ceramics International 34 (2008) 1697–1701.
[15] S. Chu, T. Yan, S. Chen, Ceramics International 26 (2000) 733–737.
[16] V. de Sousa, M. Morelli, R. Kiminami, Ceramics International 26 (2000) 561–564.
[17] C. Hwang, C. Lin, G. Wang, C. Peng, S. Chung, Journal of Alloys and Compounds 467 (2009) 514–523.
[18] C. Leach, N. Ali, D. Cupertino, R. Freer, Materials Science and Engineering B 170 (2010) 15–21.
[19] R. Subasri, M. Asha, K. Hembram, G. Rao, T. Rao, Materials Chemistry and Physics 115 (2009) 677–684.
[20] C. Chen, C. Kuo, I. Lin, Japanese Journal of Applied Physics 35 (1996) 4696–4703.
[21] B. Malecka, E. Drozdz-Ciesla, A. Malecki, Thermochimica Acta 423 (2004) 13–18.
[22] S. Marinel, M. Pollet, G. Desgardin, Journal of Materials Science-Materials in Electronics 13 (2002) 149–155.
[23] K. Mukae, K. Tsuda, I. Nagasawa, Journal of Applied Physics 50 (1979) 4475–4476.
[24] M.I. Mendelson, Journal of the American Ceramic Society 52 (1969) 443–446.
[25] H. Sawada, R. Wang, A. Sleight, Journal of Solid State Chemistry 122 (1996) 148–150.
[26] M. Inada, Japanese Journal of Applied Physics 19 (1980) 409–419.
[27] T.B. Holland, A.M. Thron, C.S. Bonifacio, A.K. Mukherjee, K. Van Benthem, Applied Physics Letters 96 (2010) 243106.
[28] Y. Jiang, Y.J. Zhu, Z.L. Xu, Materials Letters 60 (2006) 2294–2298.